Article

Phonon thermal Hall effect in a metallic spin ice

Taiki Uehara[1], Takumi Ohtsuki[2], Masafumi Udagawa[1], Satoru Nakatsuji[2,3,4] & Yo Machida [1] ✉

It has become common knowledge that phonons can generate thermal Hall effect in a wide variety of materials, although the underlying mechanism is still controversial. We study longitudinal κ_{xx} and transverse κ_{xy} thermal conductivity in $Pr_2Ir_2O_7$, which is a metallic analog of spin ice. Despite the presence of mobile charge carriers, we find that both κ_{xx} and κ_{xy} are dominated by phonons. A T/H scaling of κ_{xx} unambiguously reveals that longitudinal heat current is substantially impeded by resonant scattering of phonons on paramagnetic spins. Upon cooling, the resonant scattering is strongly affected by a development of spin ice correlation and κ_{xx} deviates from the scaling in an anisotropic way with respect to field directions. Strikingly, a set of the κ_{xx} and κ_{xy} data clearly shows that κ_{xy} correlates with κ_{xx} in its response to magnetic field including a success of the T/H scaling and its failure at low temperature. This remarkable correlation provides solid evidence that an indispensable role is played by spin-phonon scattering not only for hindering the longitudinal heat conduction, but also for generating the transverse response.

When the heat current carried by electrons is subject to a magnetic field applied normal to the current, a trajectory of electrons is curved by the Lorentz force and a transverse temperature gradient is developed in the direction both perpendicular to the heat current and the magnetic field. This phenomenon dubbed the thermal Hall effect has been believed to be restricted to materials in which there are mobile charge carriers. However, it is shown that even if the carriers of heat are neutral, the thermal Hall effect arises in several materials including magnetic insulators[1,2], multiferroics[3], spin liquid candidates[4–11], Mott insulators[12–14], and nonmagnetic insulator[15], providing new insight on heat transport in solids. In some of the preceding materials, phonons are identified as the heat carriers responsible for the thermal Hall effect[1–3,5,9,11–15]. Despite the growing number of reports presenting the phonon Hall effect, little is known about the microscopic mechanism[16–24].

To address this issue, we carried out measurements of thermal conductivity tensors in $Pr_2Ir_2O_7$, which is a kind of 'treasure trove' of attractive physical properties including Kondo effect in a frustrated magnet[25], topological Hall effect[26,27], spin ice state in a metal[27],

quantum criticality[28], and Luttinger semimetal with a quadratic band touching[29]. Among them, the relevant features to this study are the absence of a long-range magnetic order down to the lowest temperature measured and semimetallicity with low carrier density. The former prevents contamination of magnon contribution in the heat transport coefficients. While the metallicity enables precise estimation of electron contribution via the Wiedemann–Franz law, the low density of electron carriers leaves room for detection of the thermal Hall effect by chargeless carriers at the same time.

In this work, we show that longitudinal thermal conductivity κ_{xx}, in which phonon contribution by far dominates electron contribution, is largely degraded by spin–phonon scattering as low as that of amorphous silica. κ_{xx} is further lowered by the magnetic field due to resonant scattering between phonons and paramagnetic spins as evidenced by a T/H scaling. Upon cooling, magnetic fluctuations arising from spin ice correlation affect the resonant scattering by rendering another source of local level splitting through an exchange field and leads to a deviation from the T/H scaling. Despite the presence of

[1]Department of Physics, Gakushuin University, Tokyo 171-8588, Japan. [2]Institute for Solid State Physics, The University of Tokyo, Kashiwa 277-8581, Japan. [3]Department of Physics, The University of Tokyo, Tokyo 113-0033, Japan. [4]The Institute for Quantum Matter and the Department of Physics and Astronomy, The Johns Hopkins University, Baltimore, MD 21218, USA. ✉e-mail: yo.machida@gakushuin.ac.jp

mobile electrons, we detected finite thermal Hall conductivity κ_{xy} mostly generated by phonons. Unexpectedly, we find striking similarities between κ_{xx} and κ_{xy} in their response to a magnetic field, but importantly κ_{xy} behaves oppositely to κ_{xx}. This observation explicitly indicates that a single mechanism drives both longitudinal and transverse thermal response, and spin–phonon coupling which affects the mean-free path of phonons has a skew scattering component.

Results

Low longitudinal thermal conductivity in $Pr_2Ir_2O_7$

Figure 1 shows the temperature dependence of longitudinal thermal conductivity κ_{xx} of $Pr_2Ir_2O_7$ measured under zero field by applying the heat current Q parallel to the (001) plane ($Q\|(001)$). The data are shown together with those of insulating pyrochlore magnets, $Yb_2Ti_2O_7$[30], $Y_2Ti_2O_7$[31], $Dy_2Ti_2O_7$[31], and $Tb_2Ti_2O_7$[32] where heat conduction is dominated by phonons. As shown in the inset of Fig. 1a, electronic contribution $L_0\sigma_{xx}T$ to κ_{xx} estimated using the Wiedemann–Franz (WF) law is more than one order of magnitude smaller than κ_{xx} for both $Q\|(001)$ and $Q\|(111)$, which indicates that heat is predominantly transported by phonons. Interestingly, the magnitude of κ_{xx} is extremely small and approaches that of amorphous silica[33]. Moreover, the so-called phonon peak, which is characteristic of phononic thermal conductivity in insulating crystalline solids, is absent. It is shown that the structural disorder has a negligible effect on the Raman phonon spectra in the sample from the same source[34]. We thus stress that the low κ_{xx} is not due to phonon scattering by the random disorder. Since a position of the phonon peak is scaled by the Debye temperature, which is typically around 300–400 K for pyrochlore oxides[35], κ_{xx} for $Yb_2Ti_2O_7$, $Y_2Ti_2O_7$, and $Dy_2Ti_2O_7$ has the peaks at similar temperature (~10 K). At high temperatures exceeding the peak, the magnitude of thermal conductivity is set by the rate of collisions between thermally excited phonons whose number is also scaled by the Debye temperature. Thus, it is quite reasonable that κ_{xx} for $Yb_2Ti_2O_7$ and $Dy_2Ti_2O_7$ are close to each other at high temperatures.

By contrast, in $Pr_2Ir_2O_7$ the phonon peak is absent and κ_{xx} is smaller than those of $Y_2Ti_2O_7$ and $Dy_2Ti_2O_7$ by a factor of five even at high temperatures, although our samples are crystalline solids and the Debye temperature of 400 K[36] is similar to the other pyrochlore oxides. This suggests the presence of additional scatterers of phonons except for other phonons and disorders. Notably, thermal conductivity is also small and the phonon peak is absent in spin liquid candidate $Tb_2Ti_2O_7$ (Fig. 1a) where these striking features are attributed to strong phonon scattering by magnetic fluctuations[32]. As we see below, spin–phonon scattering is a leading mechanism of the low phonon thermal conductivity in $Pr_2Ir_2O_7$. An intrinsic scattering of phonon by mobile electrons may be an additional thermal impedance of the heat flow.

Resonant phonon scattering and H/T scaling

In Fig. 1b, c, magneto-thermal conductivity $\{\kappa_{xx}(H)-\kappa_{xx}(0)\}/\kappa_{xx}(0)$ are shown for $H\|[111]$ and $H\|[001]$, respectively. For both directions, κ_{xx} first decreases with field and takes a minimum. On warming, a position of minimum defined as H_{min} shifts to higher fields. (See the inset of Fig. 1c for systematic change of H_{min} with temperature for $H\|[001]$.) As shown in the inset of Fig. 1b, H_{min} increases linearly with temperature, $H_{min} \sim T$, regardless of the field directions. Such a behavior has been observed in various paramagnets and is attributed to resonant scattering between phonons and paramagnetic spins[37]. We note that this $H_{min} \sim T$ behavior is also discernible for a different sample of $Pr_2Ir_2O_7$ with larger electrical conductivity[38], indicating that our observation is an intrinsic property of heat conduction by phonons in this system. The resonance can occur in the presence of a strong spin–phonon coupling when the two-level spin systems split by the Zeeman energy absorb phonon and subsequently emit another phonon of the same energy in an unrelated direction. This spin–flip process effectively scatters phonons. The scattering becomes the largest when the Zeeman splitting $\Delta E \sim 2M\mu_B H$ (M is magnetization) is equal to phonon energy whose spectrum has a broad maximum at $\sim 4k_B T$. This causes the minimum in $\kappa_{xx}(H)$ at $H_{min} \sim 2k_B T/M\mu_B$ with H_{min} proportional to T. Therefore, field-induced change in the longitudinal thermal conductivity measured at various temperatures is expected to be scaled as a function of H/T with a minimum at $H_{min}/T \sim 2k_B/M\mu_B$. Such scaling is demonstrated in Fig. 2a, b where $\Delta\kappa_{xx}(H) = \kappa_{xx}(H)-\kappa_{xx}(0)$ normalized by its minimum value $\Delta\kappa_{xx}(H)/\kappa_{xx}^{min}$ is plotted against H/T for $H\|[111]$ and $H\|[001]$, respectively. Remarkably, all data fall onto the same curve
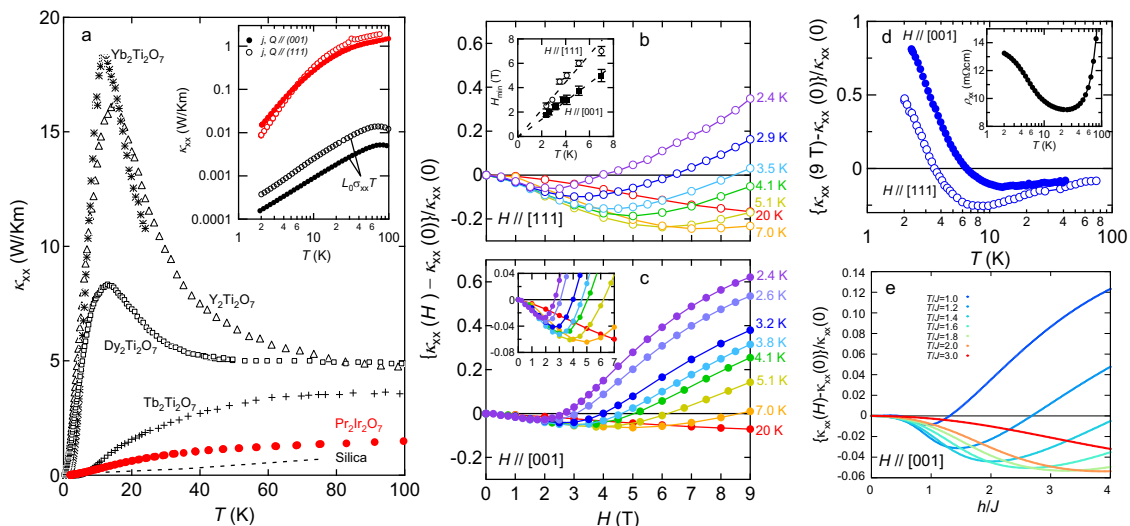

Fig. 1 | Longitudinal thermal conductivity of $Pr_2Ir_2O_7$. **a** Temperature dependence of zero-field longitudinal thermal conductivity κ_{xx} for the heat current Q parallel to the (001) plane together with those of the pyrochlore compounds[30–32]. Inset shows a κ_{xx} vs. T plot in a logarithmic scale for $Q\|(001)$ and $Q\|(111)$. The electronic contribution $L_0\sigma_{xx}T$ in κ_{xx} estimated by using the Wiedemann–Franz law is also shown for the electrical current j parallel to the (001) and (111) planes. Magnetic field dependence of longitudinal thermal conductivity normalized by the zero-field value $\{\kappa_{xx}(H)-\kappa_{xx}(0)\}/\kappa_{xx}(0)$ at different temperatures under the magnetic fields parallel to the [111] and [001] directions are shown in panels **b** and **c**, respectively. Inset of panel **b** depicts a H_{min} vs. T plot for $H\|[111]$ and $H\|[001]$. A zoom of the low field region for the $H\|[001]$ data is shown in the inset of panel **c**. **d** Temperature dependence of $\{\kappa_{xx}(H)-\kappa_{xx}(0)\}/\kappa_{xx}(0)$ at $H = 9$ T for $H\|[111]$ and $H\|[001]$. Temperature dependence of the longitudinal electrical resistivity ρ_{xx} at zero field is shown in the inset. **e** The calculated $\{\kappa_{xx}(H)-\kappa_{xx}(0)\}/\kappa_{xx}(0)$ as a function of h/J with various values of T/J for $H\|[001]$, where h is the external magnetic field and J is the nearest-neighbor interaction between Pr doublets.
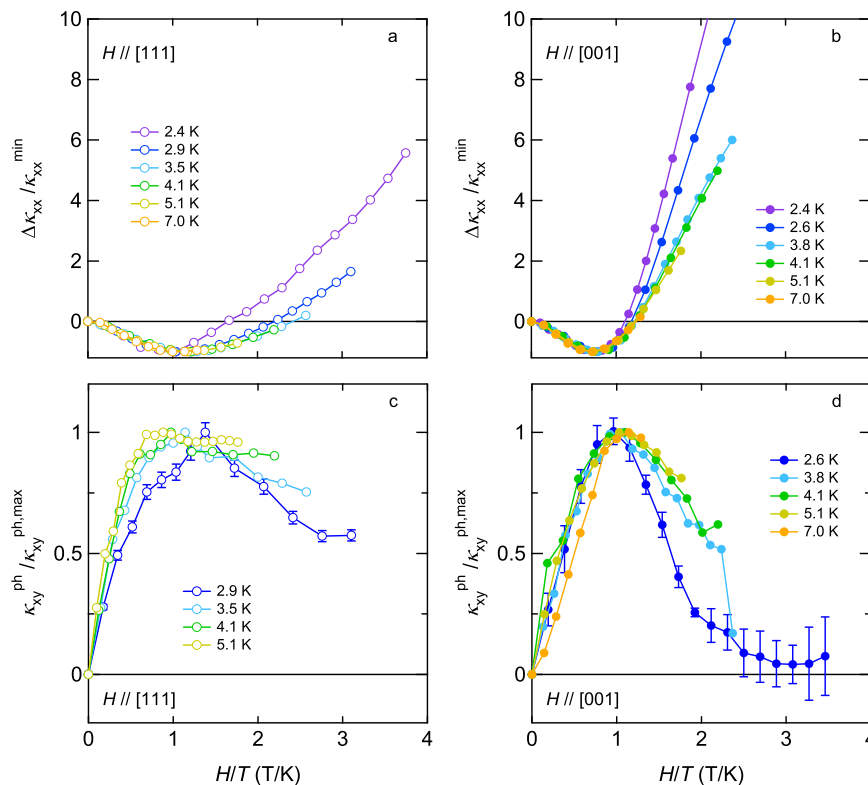
Fig. 2 | H/T scaling for longitudinal and transverse thermal conductivity.
Magnetic field-induced change in the longitudinal thermal conductivity normalized by the minimum value $\Delta\kappa_{xx}/\kappa_{xx}^{min}$ as a function of H/T for $H\|[111]$ and $H\|[001]$ are shown in panels **a** and **b**, respectively. Phonon thermal Hall conductivity normalized by the maximum value $\kappa_{xy}^{ph}/\kappa_{xy}^{ph,max}$ as a function of H/T for $H\|[111]$ and $H\|[001]$ is shown in panels **c** and **d**, respectively.

except for $H/T > 1$ and present minimum at $H/T \sim 1$. This result unambiguously indicates that $\kappa_{xx}(H)$ is controlled by the resonant phonon scattering in the region of $H < T$. For the free Pr^{3+} ion, the magnetization is expected to be $M = g_J J = 3.2$, where g_J and J represent the Landé's g factor and the total angular moment, which gives $H_{min}/T \sim 2k_B/3.2\mu_B \sim 0.93$, in good agreement with our observations. By closer looking at the data, however, one notices that the minimum position is slightly different with respect to the field directions: $H_{min}/T \sim 1.25$ and 0.75 for $H\|[111]$ and $H\|[001]$, respectively. We will come back to this point later.

Anisotropic deviation from H/T scaling and spin ice correlation
Let us turn our attention to the high field regions. With increasing field, $\{\kappa_{xx}(H)-\kappa_{xx}(0)\}/\kappa_{xx}(0)$ becomes positive (Fig. 1b, c) and the H/T scaling becomes failed (Fig. 2a, b). Concomitantly, we resolved a clear anisotropy in $\{\kappa_{xx}(H)-\kappa_{xx}(0)\}/\kappa_{xx}(0)$, especially at low temperatures: while $\{\kappa_{xx}(H)-\kappa_{xx}(0)\}/\kappa_{xx}(0)$ for $H\|[111]$ increases with a concave curvature, the one for $H\|[001]$ increases with a convex curvature and shows a tendency to saturate at low temperatures. Since the resonant scattering between phonons and paramagnetic spins is responsible for the negative magneto-thermal conductivity, the observed anisotropic recovery of $\kappa_{xx}(H)$ implies the magnitude of resonant scattering is substantially influenced by spin correlation.

In magnetic materials, magnetic fluctuations yield strong scattering on phonons and significantly suppress phononic heat conduction[39]. An application of a magnetic field, however, weakens magnetic fluctuations and leads to a striking enhancement of phonon thermal conductivity[30,32,40]. The observed response of κ_{xx} to magnetic fields can be understood based on this line of thought. In particular, anisotropic magneto-thermal conductivity explicitly indicates a vital role of phonon scattering by fluctuating spins with spin ice correlation. In spin ice state[41], the spin system fluctuates between the energetically equivalent "2-in, 2-out" configurations within the ground state

manifold. This gives rise to strong magnetic fluctuations. The macroscopic degeneracy is lifted by the external magnetic field in an anisotropic way[42,43]. Magnetic field along the [001] direction steeply lifts the ground state degeneracy and suppresses the magnetic fluctuations because the stable spin configuration is uniquely determined as one of the six equivalent "2-in, 2-out" configurations by the field. For $H\|[111]$, "3-in, 1-out/1-in, 3-out" configuration is energetically favored in high field limit. However, due to a smaller Zeeman energy gain for the spins on the Kagome plane with the "3-in, 1-out/1-in, 3-out" configuration than the "2-in, 2-out" configuration, the system remains in spin ice manifold and preserves the strong magnetic fluctuations up to higher field[44,45].

This anisotropic suppression of magnetic fluctuations brings about positive and anisotropic magneto-thermal conductivity. For $H\|[001]$, the steep suppression of the magnetic fluctuations yields the rapid rise of $\{\kappa_{xx}(H)-\kappa_{xx}(0)\}/\kappa_{xx}(0)$ (Fig. 1c). Once the polarized state with the "2-in, 2-out" configuration is stabilized by the fields and fluctuations are totally suppressed, κ_{xx} gets saturated to a value which is purely dominated by phonons. Namely, the resonant scattering does not work anymore, since the spins are fully polarized in a saturation field, and the number of phonons carrying sufficient energy to flip the spin is exponentially suppressed. Meanwhile, the persistence of the magnetic fluctuations for $H\|[111]$ yields the slower rise of $\{\kappa_{xx}(H)-\kappa_{xx}(0)\}/\kappa_{xx}(0)$ (Fig. 1b).

Figure 1d shows temperature dependence of $\{\kappa_{xx}(H)-\kappa_{xx}(0)\}/\kappa_{xx}(0)$ measured at 9 T for $H\|[111]$ and $H\|[001]$. On cooling, $\{\kappa_{xx}(H)-\kappa_{xx}(0)\}/\kappa_{xx}(0)$ changes a sign from negative to positive around 4 and 7 K for $H\|[111]$ and $H\|[001]$, respectively. As mentioned above, the resonant phonon scattering is strongly influenced by spin correlation through a local exchange field. However, by applying a large magnetic field, or equivalently at low temperatures, the local spin splitting becomes mainly determined by an external magnetic field. This crossover causes a gradual change from negative to positive magneto-thermal conductivity. In that sense, the sign-change temperature can

be regarded as a lower bound of onset temperature below which the spin-ice correlation sets in. Notably, this temperature roughly coincides with a resistivity minimum (see the inset of Fig. 1d) which is another consequence of the spin-ice correlation while in this case, the correlated spins interact with conduction electrons[46].

Now, let us discuss the implication of the spin-ice correlations to the anisotropy in H_{min}. Under the spin ice state, the Zeeman splitting $\Delta E \sim 2M\mu_B H$ of the ground state doublet is anisotropic with respect to the field directions due to anisotropy in magnetization M[25]. Accordingly, given the relation of $H_{min} \sim 2k_B T/M\mu_B$, H_{min} is anisotropic and its anisotropic ratio between [111] and [001] directions is expected to be held a relation of $H_{min}^{[111]}/H_{min}^{[001]} \sim M_{[001]}/M_{[111]}$. This means that at a given temperature the larger Zeeman splitting ΔE due to the larger M satisfies the condition of resonance at the lower field. In fact, the anisotropic ratio of H_{min}, $(H_{min}^{[111]}/T)/(H_{min}^{[001]}/T) = 1.25/0.75 \sim 1.67$ extracted from Fig. 2a, b, is in good agreement with magnetization anisotropy expected for the "2-in, 2-out" configuration, $M_{[001]}/M_{[111]} = \{g_J J(1/\sqrt{3})\}/\{g_J J(1 + 1/3 \times 1)/4\} \sim 1.73$.

Our argument that the spin–phonon scattering controls the evolution of $\kappa_{xx}(H)$ is supported by a theoretical calculation. We model the interaction between the Pr doublets by a simple spin-ice-type Ising model. What is characteristic of this compound is the spin–phonon interaction: we assume a linear transverse coupling between the Pr doublets and acoustic phonons. The Pr^{3+} ion takes f^2 configurations in $Pr_2Ir_2O_7$, and its single-ion ground state is described as a non-Kramers doublet taking E_g representation in a D_{3d} symmetric local crystal field[47,48]. In this case, the local transverse component of the doublet has quadrupole nature, which enables the linear coupling to lattice deformations or phonons. Even within this simple model, we can qualitatively reproduce main experimental features of magneto-thermal transport as shown in Fig. 1e; the initial negative magneto-thermal conductivity, the presence of minimum, and the positive increase with the convex curvature at the low temperature and a high field region.

Here we note the role of magnetic excitations in thermal transport. In spin ice, magnetic monopoles are excited above the temperature of the order of exchange coupling. Indeed, the dynamics and transport of monopoles are widely discussed both experimentally and theoretically. However, in $Pr_2Ir_2O_7$, we can safely ignore their contribution. Since the magnetic field applied along the [001] direction is unfavorable for the spin ice state, the number of monopoles decays faster for $H\|[001]$ than $H\|[111]$. Therefore, if heat is carried by the monopoles, $\kappa_{xx}(H)$ is expected to fall rapidly for $H\|[001]$ than $H\|[111]$. This is indeed observed in $Yb_2Ti_2O_7$[30], and they raised this behavior as the major evidence for monopole transport. However, in our system, $\kappa_{xx}(H)$ falls rapidly for $H\|[111]$. This observation clearly shows that monopoles do not play a major role in the thermal transport in the measured temperature range. To raise one more evidence for the irrelevancy of monopoles, the reduction of $\kappa_{xx}(H)$ with the field is observed up to as high as 80 K (Fig. 1d), which is much higher than the characteristic temperature of spin ice correlations.

Thermal Hall effect by phonons
Having established the dominant role of spin–phonon scattering in the longitudinal thermal conductivity, let us focus on the thermal Hall effect. Temperature dependence of thermal Hall conductivity divided by temperature κ_{xy}/T measured under magnetic field of 9 T for $H\|[111]$ and $H\|[001]$ are shown in Fig. 3a, b, respectively. In the same figures, we also show the electronic contribution $L_0\sigma_{xy}$ (left axis) and κ_{xx}/T (right axis). Surprisingly, a sign of $L_0\sigma_{xy}$ is opposite to κ_{xy}/T in the whole measured temperature range for $H\|[111]$ and $T > 4$ K for $H\|[001]$, indicating that the thermal Hall effect is mostly governed by carriers except for electrons. Given the negligible contribution of monopoles in κ_{xx}, they are not responsible for the Hall response either. Thus, phonons are most probably the unique heat carriers that can cause thermal Hall effect in this paramagnet. Moreover, both κ_{xy}/T and κ_{xx}/T

peak around 20–30 K where phonons dominate the longitudinal thermal conductivity because electron contribution accounts for only $L_0\sigma_{xy}T/\kappa_{xx} \sim 0.6\%$ of the total κ_{xx} (see the inset of Fig. 1a). Such a coincidence of peaks in κ_{xx} and κ_{xy} has been observed in several insulating solids and regarded as a clue to identify the thermal Hall signal generated by phonons[15]. This result further supports the conjecture that thermal Hall current is carried by phonons in $Pr_2Ir_2O_7$. We note a ratio $\kappa_{xy}/\kappa_{xx} \simeq 0.4\text{–}0.8 \times 10^{-3}$ around the peak is comparable to that found in materials where phonons have been argued to cause the Hall effect[2,11].

At temperatures above the peak, the magnitude of κ_{xy}/T is comparable with that of $Tb_2Ti_2O_7$[4] and smaller than the unexpectedly large thermal Hall conductivity of $SrTiO_3$[15] and La_2CuO_4[12] by a factor of 10 (the inset of Fig. 3b). Below the peak, κ_{xy}/T steeply decreases faster than κ_{xx}/T. κ_{xy}/T for $H\|[001]$ seems to approach the value expected from the WF law followed by a sign change around 4 K, showing that phonons cease to contribute to the Hall response at low temperatures.

In Fig. 3c, d, we show magnetic field dependence of thermal Hall conductivity $\kappa_{xy}(H)$ (triangles) together with electron contribution $L_0\sigma_{xy}T(H)$ (dotted lines) estimated by using the WF law for $H\|[111]$ and $H\|[001]$, respectively. Again, a sign of $L_0\sigma_{xy}T(H)$ is opposite to κ_{xy}. By subtracting $L_0\sigma_{xy}T(H)$ from $\kappa_{xy}(H)$, we evaluated thermal Hall conductivity generated by phonons as $\kappa_{xy}^{ph} = \kappa_{xy} - L_0\sigma_{xy}T$ (circles). As seen from the figures, at 20 K $\kappa_{xy}(H)$ increases linearly with H and there is negligible electron contribution in both directions. On cooling, $\kappa_{xy}(H)$ becomes non-monotonic. Namely, $\kappa_{xy}(H)$ shows a peak and subsequently decreases with the field. Moreover, a fraction of the electron contribution to κ_{xy} slightly increases, which is maximized up to $|L_0\sigma_{xy}T|/\kappa_{xy} \sim 28\%$ at 2.9 K and $H = 4$ T$\|[111]$. Since the peak remains in $\kappa_{xy}^{ph}(H)$ even after the subtraction of electron contribution, phonons are responsible for the non-monotonic behavior. By further decreasing temperature, an anisotropic field response emerges at high fields. $\kappa_{xy}(H)$ for $H\|[001]$ is considerably suppressed above its peak field and approaches a value expected from the WF law within an experimental error (the inset of Fig. 3d), consistent with what we saw in the temperature variation of κ_{xy}/T (Fig. 3b). By contrast, the suppression is weak for $H\|[111]$ and $\kappa_{xy}^{ph}(H)$ remains positive up to 9 T.

Correlation between κ_{xx} and κ_{xy}
One of the most striking findings of this work is a correlation between field-induced change in κ_{xy}^{ph} and κ_{xx}, which are displayed in the upper and lower panels of Fig. 4, respectively. In each panel, we compare two data taken at the (nearly) same temperature for $H\|[111]$ (open circles) and for $H\|[001]$ (closed circles). In Fig. 4, there are several things of interest. (i) The maximum and the minimum appear at nearly the same field in $\kappa_{xy}^{ph}(H)$ and $\Delta\kappa_{xx}(H)$, respectively, and the extreme positions shift to a lower field with decreasing temperature. (ii) Above 7 K, the relationship in the magnitude of $\Delta\kappa_{xx}(H)$ between the two directions is the same as $\kappa_{xy}^{ph}(H)$: the large negative magneto-thermal conductivity is accompanied by the large thermal Hall signal for $H\|[111]$, and vice versa for $H\|[001]$. (iii) Below 5.1 K, steeper $\Delta\kappa_{xx}(H)$ rises above its minimum field, stronger the suppression of $\kappa_{xy}^{ph}(H)$ becomes above its maximum field. Upon cooling, this correlation becomes more significant for $H\|[001]$.

From the observation (i), the striking resemblance between $\kappa_{xy}^{ph}(H)$ and $\Delta\kappa_{xx}(H)$ led us to expect that the H/T scaling is also valid for $\kappa_{xy}^{ph}(H)$. As demonstrated in Fig. 2c, d, the data of $\kappa_{xy}^{ph}(H)$ divided by its maximum value indeed collapse on a single curve for both directions for $H/T < 1$ as in the case of $\kappa_{xx}(H)$ (Fig. 2a, b). Moreover, observation (ii) indicates that the strong paramagnetic scattering of phonons that gives rise to the negative magneto-thermal conductivity is an ingredient to enhance the phonon thermal Hall effect. These results provide compelling evidence that a prominent role is played by resonant phonon scattering not only in degrading longitudinal phonon heat conduction but also in generating the transverse signal.

We note that the scaling of κ_{xy}^{ph} also becomes failed for $H/T > 1$ (Fig. 2c, d), indicating that the paramagnetic scattering no longer plays a
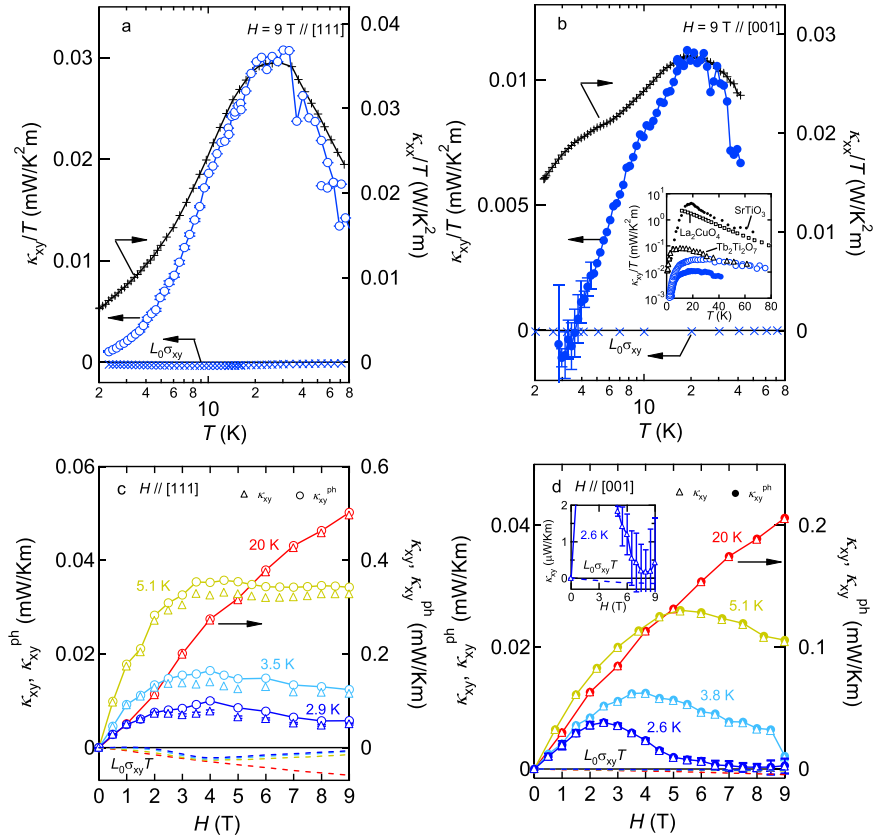
Fig. 3 | Thermal Hall conductivity of Pr₂Ir₂O₇. Temperature dependence of thermal Hall conductivity divided by temperature κ_{xy}/T and $L_0\sigma_{xy}$ (left axis) together with longitudinal thermal conductivity divided by temperature κ_{xx}/T (right axis) under the magnetic field of 9 T applied parallel to the [111] and [001] directions are shown in panels **a** and **b**, respectively. In the inset of panel **b**, our data are compared with those of Tb₂Ti₂O₇[4], SrTiO₃[15], and cuprate Mott insulator[12]. Magnetic field dependence of κ_{xy} (triangles) and $L_0\sigma_{xy}T$ (dotted lines) at different temperatures for $H\|$[111] and $H\|$[001] are shown in panels **c** and **d**, respectively. Phonon contribution estimated by $\kappa_{xy}^{ph} = \kappa_{xy} - L_0\sigma_{xy}T$ is also shown by circles. κ_{xy} for $H\|$[001] seems to approach the $L_0\sigma_{xy}T$ value at high fields as displayed in the inset of panel (**d**).

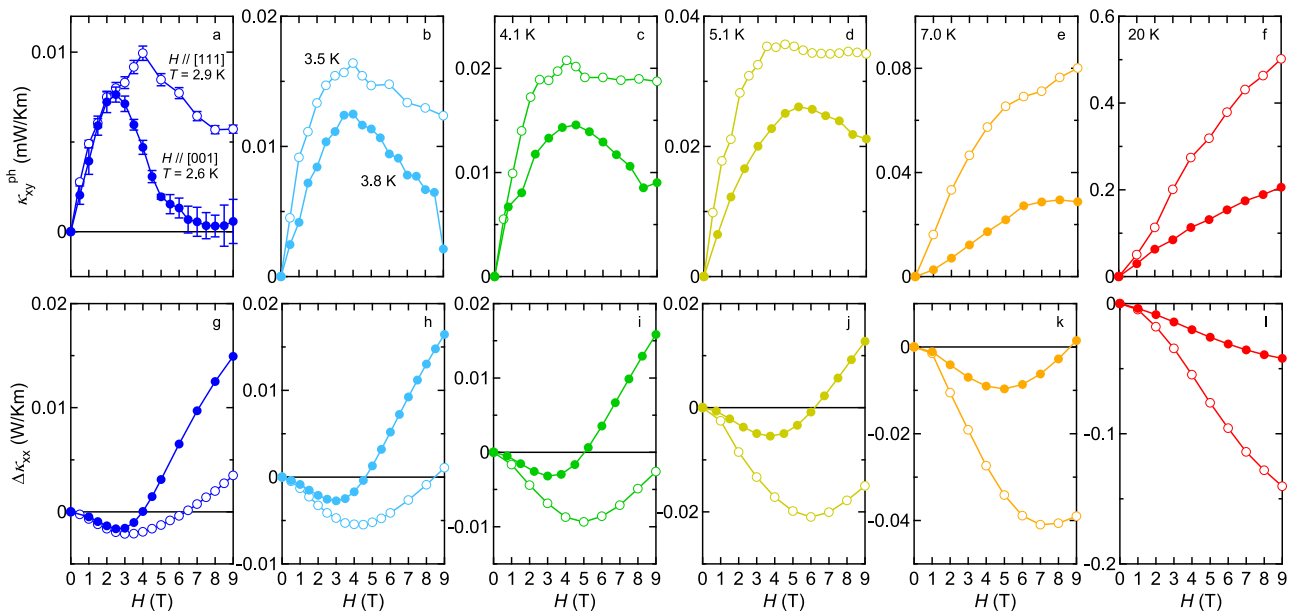**Fig. 4 | Correlation between longitudinal and transverse thermal conductivity.** Magnetic field dependence of thermal Hall conductivity of phonons κ_{xy}^{ph} (upper panels) and magnetic field-induced change in the longitudinal thermal conductivity $\Delta\kappa_{xx} = \kappa_{xx}(H) - \kappa_{xx}(0)$ (lower panels) for $H\|$[111] (open circles) and $H\|$[001] (closed circles). In panels **a** and **g**, measurements are performed at $T = 2.9$ and 2.6 K for $H\|$[111] and $H\|$[001], respectively. **b**, **h** $T = 3.5$ and 3.8 K for $H\|$[111] and $H\|$[001], respectively, **c**, **i** 4.1 K, **d**, **j** 5.1 K, **e**, **k** 7.0 K, and **f**, **l** 20 K.

major role in this regime. Instead, from the remarkable correlation in the observation (iii), it is quite natural to identify another source of asymmetric scattering of phonons as magnetic fluctuations. Whereas the survival of magnetic fluctuations along the [111] direction yields the sizable $\kappa_{xy}^{\mathrm{ph}}$ even after the paramagnetic scattering dies out, the strong suppression of magnetic fluctuations along the [001] direction results in the substantial decrease of κ_{xy} towards the value purely dominated by electrons. Thus, it is concluded that whatever the spin state is (whether spins are paramagnetic or correlated) when phonons interact with spins, they are asymmetrically scattered and produce the thermal Hall signal.

To attempt to clarify the intriguing thermal Hall phenomena in $Pr_2Ir_2O_7$, one should seriously take into account the following two facts. First, the evolution of κ_{xx} with the field can be thoroughly explained by the way spins scatter phonons. This indicates an intrinsic coupling of phonons to the magnetic environment. Second, there is a manifest correlation between κ_{xx} and κ_{xy} in their evolution within the field. These two facts impose constraints on possible scenarios that the longitudinal and transverse thermal responses should be understood in a unified way in terms of an intrinsic coupling of phonons to spins with a skew component and make a possibility of the extrinsic origin like the skew scattering of phonons by superstoichiometric rare-earth ions[20], oxygen vacancies[23], and dynamical defects[24] unlikely.

Methods

Samples
Single crystals of $Pr_2Ir_2O_7$ were grown by a flux method[49]. We used two different single crystals for the thermal transport measurements under a magnetic field applied parallel to the [111] and [001] directions. The [111] ($H\|[111]$) and [001] ($H\|[001]$) samples have plate-like shape with dimensions of $1.7(\text{width}) \times 2.1 \,(\text{length})\,\mathrm{mm}^2$ in the (111) plane and $1.1(\text{width}) \times 2.1(\text{length})\,\mathrm{mm}^2$ in the (001) plane, respectively. The thicknesses of the samples are about 0.5 mm.

Thermal transport measurements
Longitudinal thermal conductivity κ_{xx} and thermal Hall conductivity κ_{xy} were measured by the standard steady-state method in a high vacuum. The heat flow Q was injected in the (111) and (001) planes for the [111] and [001] samples, respectively, by heating a chip resistor attached to one end of the sample. The other end of the sample was attached to an insulating LiF plate, which was used as a cold thermal bath. The longitudinal ΔT_x and transverse ΔT_y temperature differences were determined by Cernox thermometers. The thermometers and the heater were connected by gold wires ($\varnothing = 25\,\mu\mathrm{m}$) and heat-cured silver paint (Dupont 6838) to the sample. The contact resistances were $10\,\mathrm{m}\Omega$. To remove the longitudinal response from the raw data due to misalignment of the contacts, we anti-symmetrized it as $\Delta T_y(H) = \{\Delta T_y(+H) - \Delta T_y(-H)\}/2$. κ_{xx} and κ_{xy} were obtained from the longitudinal thermal resistivity, $w_{xx} = (\Delta T_x/Q)(wt/l)$, and the thermal Hall resistivity, $w_{xy} = (\Delta T_y/Q)t$, as $\kappa_{xx} = w_{xx}/(w_{xx}^2 + w_{xy}^2)$ and $\kappa_{xy} = -w_{xy}/(w_{xx}^2 + w_{xy}^2)$. Here, l, w, and t are lengths between the contacts, width, and thickness of the samples, respectively. The electrical (Hall) resistivity measurements were done by using the same contacts and gold wires. κ_{xx} and κ_{xy} were checked to be independent of the thermal gradient by changing $\Delta T_x/T$ in the range of 1–20%. Since ΔT_y is tiny, which is as small as 0.1 mK, at low temperatures and the scattering of the data is large, the measurements were repeated several times and the data is averaged. Error bars in the main figures represent one standard deviation.

Computational
Here, we summarize a theoretical formulation to calculate the longitudinal thermal conductivity of acoustic phonons, as shown in Fig. 1e. We assume two kinds of scattering centers, non-magnetic impurities and localized Pr moments. The former gives a scattering rate weakly dependent on the energy of phonons, which results in the normal $\propto T^3$ behavior of phonon thermal conductivity in the low-temperature limit.

The latter scattering process is characteristic of this system, in particular, the non-Kramers nature of Pr moments. It was pointed out that the transverse components of Pr doublets behave as magnetic quadrupoles rather than dipoles in the Pr pyrochlore oxides[47,48]. Consequently, the lattice deformation couples to the transverse components of Pr doublets, or conversely, the acoustic phonons are scattered inelastically through the flip of Pr doublets.

Combining these two types of scattering processes, the thermal conductivity can be concisely written as

$$\kappa_{xx} = \kappa_0 \left(1 - \frac{\delta}{T^5} \frac{1}{N} \sum_j \frac{\Delta_j^4}{\sinh^2 \frac{\Delta_j}{2T}} \right), \tag{1}$$

where $\kappa_0 \equiv \frac{2\pi^2 \tau T^3}{15c}$ is the normal phonon thermal conductivity. Δ_j is the splitting of Pr doublet at site j due to the "local effective field", i.e. the combined effects of the external magnetic field and the exchange interaction with surrounding doublets. δ is the variance of the local effective field, which is essential to the resonant spin–phonon scattering and is usually attributed to the randomness in the system.

In the present analysis, we adopt the nearest-neighbor spin ice model to describe the thermal fluctuation of Pr doublets,

$$\mathcal{H} = J \sum_{\langle j,j' \rangle} \sigma_j \sigma_{j'} - \mathbf{h} \cdot \sum_j \sigma_j \mathbf{d}_j. \tag{2}$$

Here the first term is the nearest-neighbor interaction between Pr doublets, $\sigma_j = \pm 1$. The second term describes the site-dependent Zeeman interaction with the external magnetic field, $\mathbf{h}$. $\mathbf{d}_j$ stands for the easy axis of the Pr doublet at site j. We assume the case of [001] field direction, and conducted the Monte Carlo simulation for $N = 16 \times 16 \times 16 \times 4 = 16{,}384$ doublets and, made 10,000 samplings for the effective field, $\Delta_j \equiv (\frac{2}{\sqrt{3}}h - 2J\sum_{j'}\sigma_{j'})\sigma_j$. From the thermal average, we obtain the thermal conductivity through Eq. (1).

Data availability
The data that support the findings of this study are available from the corresponding author upon reasonable request.

References

1. Strohm, C., Rikken, G. L. J. A. & Wyder, P. Phenomenological evidence for the phonon Hall effect. *Phys. Rev. Lett.* **95**, 155901 (2005).
2. Chen, L., Boulanger, M.-E., Wang, Z.-C., Tafti, F. & Taillefer, L. Large phonon thermal Hall conductivity in a simple antiferromagnetic insulator. Preprint at http://arxiv.org/abs/2110.13277 (2021).
3. Ideue, T., Kurumaji, T., Ishiwata, S. & Tokura, Y. Giant thermal Hall effect in multiferroics. *Nat. Mater.* **16**, 797–802 (2017).
4. Hirschberger, M., Krizan, J. W., Cava, R. J. & Ong, N. P. Large thermal Hall conductivity of neutral spin excitations in a frustrated quantum magnet. *Science* **348**, 106–109 (2015).
5. Sugii, K. et al. Thermal Hall effect in a phonon-glass $Ba_3CuSb_2O_9$. *Phys. Rev. Lett.* **118**, 145902 (2017).
6. Kasahara, Y. et al. Unusual thermal Hall effect in a Kitaev spin liquid candidate α-$RuCl_3$. *Phys. Rev. Lett.* **120**, 217205 (2018).
7. Kasahara, Y. et al. Majorana quantization and half-integer thermal quantum Hall effect in a Kitaev spin liquid. *Nature* **559**, 227–231 (2018).
8. Hentrich, R. et al. Large thermal Hall effect in α-$RuCl_3$: evidence for heat transport by Kitaev–Heisenberg paramagnons. *Phys. Rev. B* **99**, 085136 (2019).
9. Akazawa, M. et al. Thermal Hall effects of spins and phonons in Kagome antiferromagnet Cd-Kapellasite. *Phys. Rev. X* **10**, 041059 (2020).
10. Yokoi, T. et al. Half-integer quantized anomalous thermal Hall effect in the Kitaev material candidate α-$RuCl_3$. *Science* **373**, 568–572 (2021).

11. Lefrançois, É. et al. Evidence of a phonon Hall effect in the Kitaev spin liquid candidate α-RuCl$_3$. *Phys. Rev. X* **12**, 021025 (2022).

12. Grissonnanche, G. et al. Giant thermal Hall conductivity in the pseudogap phase of cuprate superconductors. *Nature* **571**, 376–380 (2019).

13. Grissonnanche, G. et al. Chiral phonons in the pseudogap phase of cuprates. *Nat. Phys.* **16**, 1108–1111 (2020).

14. Boulanger, M.-E. et al. Thermal Hall conductivity in the cuprate Mott insulators Nd$_2$CuO$_4$ and Sr$_2$CuO$_2$Cl$_2$. *Nat. Commun.* **11**, 5325 (2020).

15. Li, X., Fauqué, B., Zhu, Z. & Behnia, K. Phonon thermal Hall effect in strontium titanate. *Phys. Rev. Lett.* **124**, 105901 (2020).

16. Sheng, L., Sheng, D. N. & Ting, C. S. Theory of the phonon Hall effect in paramagnetic dielectrics. *Phys. Rev. Lett.* **96**, 155901 (2006).

17. Wang, J.-S. & Zhang, L. Phonon Hall thermal conductivity from the Green–Kubo formula. *Phys. Rev. B* **80**, 012301 (2009).

18. Zhang, L., Ren, J., Wang, J.-S. & Li, B. Topological nature of the phonon Hall effect. *Phys. Rev. Lett.* **105**, 225901 (2010).

19. Qin, T., Zhou, J. & Shi, J. Berry curvature and the phonon Hall effect. *Phys. Rev. B* **86**, 104305 (2012).

20. Mori, M., Spencer-Smith, A., Sushkov, O. P. & Maekawa, S. Origin of the phonon Hall effect in rare-earth garnets. *Phys. Rev. Lett.* **113**, 265901 (2014).

21. Saito, T., Misaki, K., Ishizuka, H. & Nagaosa, N. Berry phase of phonons and thermal Hall effect in nonmagnetic insulators. *Phys. Rev. Lett.* **123**, 255901 (2019).

22. Yang, Y.-F., Zhang, G.-M. & Zhang, F.-C. Universal behavior of the thermal Hall conductivity. *Phys. Rev. Lett.* **124**, 186602 (2020).

23. Flebus, B. & MacDonald, A. H. Charged defects and phonon Hall effects in ionic crystals. *Phys. Rev. B* **105**, L220301 (2022).

24. Sun, X.-Q., Chen, J.-Y. & Kivelson, S. A. Large extrinsic phonon thermal Hall effect from resonant scattering. Preprint at http://arxiv.org/abs/2109.12117 (2021).

25. Nakatsuji, S. et al. Metallic spin-liquid behavior of the geometrically frustrated Kondo lattice Pr$_2$Ir$_2$O$_7$. *Phys. Rev. Lett.* **96**, 087204 (2006).

26. Machida, Y. et al. Unconventional anomalous Hall effect enhanced by a noncoplanar spin texture in the frustrated Kondo lattice Pr$_2$Ir$_2$O$_7$. *Phys. Rev. Lett.* **98**, 057203 (2007).

27. Machida, Y., Nakatsuji, S., Onoda, S., Tayama, T. & Sakakibara, T. Time-reversal symmetry breaking and spontaneous Hall effect without magnetic dipole order. *Nature* **463**, 210–213 (2010).

28. Tokiwa, Y., Ishikawa, J. J., Nakatsuji, S. & Gegenwart, P. Quantum criticality in a metallic spin liquid. *Nat. Mater.* **13**, 356–359 (2014).

29. Kondo, T. et al. Quadratic Fermi node in a 3D strongly correlated semimetal. *Nat. Commun.* **6**, 10042 (2015).

30. Tokiwa, Y. et al. Possible observation of highly itinerant quantum magnetic monopoles in the frustrated pyrochlore Yb$_2$Ti$_2$O$_7$. *Nat. Commun.* **7**, 10807 (2016).

31. Kolland, G., Valldor, M., Hiertz, M., Frielingsdorf, J. & Lorenz, T. Anisotropic heat transport via monopoles in the spin-ice compound Dy$_2$Ti$_2$O$_7$. *Phys. Rev. B* **88**, 054406 (2013).

32. Li, Q. J. et al. Phonon-glass-like behavior of magnetic origin in single-crystal Tb$_2$Ti$_2$O$_7$. *Phys. Rev. B* **87**, 214408 (2013).

33. Keller, R. C. & Pohl, R. O. Thermal conductivity and specific heat of noncrystalline solids. *Phys. Rev. B* **4**, 2029 (1971).

34. Xu, Y. et al. Phonon spectrum of Pr$_2$Zr$_2$O$_7$ and Pr$_2$Ir$_2$O$_7$ as evidence of coupling of the lattice with electronic and magnetic degrees of freedom. *Phys. Rev. B* **105**, 075137 (2022).

35. Subramanian, M. A., Aravamudan, G. & Rao, G. V. S. Oxide pyrochlores—a review. *Prog. Solid State Chem.* **15**, 55–143 (1983).

36. Ghosh, B. & Mukhopadhyay, S. Unified description of resistivity and thermopower of Pr$_2$Ir$_2$O$_7$: possible influence of crystal field excitation in a Kondo lattice. *Phys. Rev. B* **103**, 165135 (2021).

37. Berman, R. *Thermal Conduction in Solids* (Clarendon Press, Oxford, 1976).

38. Ni, J. M. et al. Giant isotropic magneto-thermal conductivity of metallic spin liquid candidate Pr$_2$Ir$_2$O$_7$ with quantum criticality. *Nat. Commun.* **12**, 307 (2021).

39. Sharma, P. A. et al. Thermal conductivity of geometrically frustrated, ferroelectric YMnO$_3$: extraordinary spin–phonon interactions. *Phys. Rev. Lett.* **93**, 177202 (2004).

40. Wang, X. M. et al. Large magnetothermal conductivity of HoMnO$_3$ single crystals and its relation to the magnetic-field-induced transitions of magnetic structure. *Phys. Rev. B* **82**, 094405 (2010).

41. Udagawa, M. & Jaubert, L. (eds) *Spin Ice. Springer Series in Solid-State Sciences* (Springer, Cham, 2021).

42. Fukazawa, H., Melko, R. G., Higashinaka, R., Maeno, Y. & Gingras, M. J. P. Magnetic anisotropy of the spin-ice compound Dy$_2$Ti$_2$O$_7$. *Phys. Rev. B* **65**, 054410 (2002).

43. Hiroi, Z., Matsuhira, K., Takagi, S., Tayama, T. & Sakakibara, T. Specific heat of Kagomé ice in the pyrochlore oxide Dy$_2$Ti$_2$O$_7$. *J. Phys. Soc. Jpn.* **72**, 411–418 (2003).

44. Udagawa, M., Ogata, M. & Hiroi, Z. Exact result of ground-state entropy for Ising pyrochlore magnets under a magnetic field along [111] axis. *J. Phys. Soc. Jpn.* **71**, 2365–2368 (2002).

45. Moessner, R. & Sondhi, S. L. Theory of the [111] magnetization plateau in spin ice. *Phys. Rev. B* **68**, 064411 (2003).

46. Udagawa, M., Ishizuka, H. & Motome, Y. Non-Kondo mechanism for resistivity minimum in spin ice conduction systems. *Phys. Rev. Lett.* **108**, 066406 (2012).

47. Onoda, S. & Tanaka, Y. Quantum fluctuations in the effective pseudospin-$\frac{1}{2}$ model for magnetic pyrochlore oxides. *Phys. Rev. B* **83**, 094411 (2011).

48. Rau, J. G. & Gingras, M. J. P. Frustrated quantum rare-earth pyrochlores. *Annu. Rev. Condens. Mater.* **10**, 357–386 (2019).

49. Millican, J. N. et al. Crystal growth and structure of R_2Ir$_2$O$_7$ (R = Pr, Eu) using molten KF. *Mater. Res. Bull.* **42**, 928–934 (2007).

Author contributions

Y.M. conceived and designed the study. T.U. and Y.M. performed the transport measurements and analyzed the data. T.O. and S.N. synthesized the single crystal samples. M.U. performed the theoretical calculations. Y.M. and M.U. wrote the manuscript.

Competing interests

The authors declare no competing interests.

Additional information

Correspondence and requests for materials should be addressed to Yo Machida.

Peer review information *Nature Communications* thanks Zhaoming Tian, Yi-feng Yang and the other, anonymous, reviewer for their contribution to the peer review of this work.

Reprints and permission information is available at http://www.nature.com/reprints

Publisher's note Springer Nature remains neutral with regard to jurisdictional claims in published maps and institutional affiliations.